
Optical Lattices: Theory

A. Smerzi¹ and A. Trombettoni²

¹ Istituto Nazionale per la Fisica della Materia BEC-CRS and Dipartimento di Fisica, Universita' di Trento, I-38050 Povo, Italy. smerzi@science.unitn.it

² International School for Advanced Studies and Sezione INFN, Via Beirut 2/4, I-34104, Trieste, Italy. andreatr@sissa.it

1 Introduction

This chapter presents an overview of the properties of a Bose-Einstein condensate (BEC) trapped in a periodic potential. This system has attracted a wide interest in the last years, and a few excellent reviews of the field have already appeared in the literature (see, for instance, [1, 2, 3] and references therein). For this reason, and because of the huge amount of published results, we do not pretend here to be comprehensive, but we will be content to provide a flavor of the richness of this subject, together with some useful references. On the other hand, there are good reasons for our effort. Probably, the most significant is that BEC in periodic potentials is a truly interdisciplinary problem, with obvious connections with electrons in crystal lattices, polarons and photons in optical fibers. Moreover, the BEC experimentalists have reached such a high level of accuracy to create in the lab, so to speak, paradigmatic Hamiltonians, which were first introduced as idealized theoretical models to study, among others, dynamical instabilities or quantum phase transitions.

The key feature of our problem is that the periodic potential naturally introduce a spatial *discreteness* in a nonlinear medium. The periodic potential is generally realized with two counterpropagating laser beams [4, 5, 6, 7, 8, 9, 10, 11, 12], so as to create an optical lattice (OL). As expected in the mean-field GPE limit, the BEC Bogoliubov excitation spectrum has a band structure, in analogy with the electronic Bloch bands [13, 14, 15, 16, 17, 18, 19, 20, 21]. When the the power of the laser is fairly larger than the chemical potential, the lowest band dynamics maps on a discrete nonlinear Schrödinger (DNLS) equation [22]. This was an interesting remark especially because the DNLS was already widely investigated *per se* by the nonlinear physics community [23, 24, 25] which, indeed, was immediately attracted by the new possibilities offered by this system.

The BEC GPE dynamics in the array can be therefore studied in the framework of the nonlinear lattice theory [22, 26, 27, 28]. The typical confining potential is given by the superposition of an harmonic trap and a periodic potential. For a 1D OL, the frequency at the bottom of the wells is typically of order of $\sim kHz$

in the OL direction, and the transverse confinement is provided by the magnetic potential (characterized by frequencies of order of $100Hz$). The axial dynamics of a Bose condensate induced by an external potential with cylindrical symmetry in the transverse directions can be studied introducing an effective $1D$ GPE equation [29]: for BEC in OL, assuming that the Wannier wavefunctions (localized in each well) can be expressed in Thomas-Fermi approximation, it has been shown [30] that the main effect of the transverse confinement is to modify the degree of non-linearity of the DNLS equation, giving raise to a generalized version of the DNLS equation. BEC in a periodic potential can allow for the observation of intrinsic localized modes (i.e. matter excitations localized on few lattice sites), as well as the study of solitons and breathers, possibly also with condensates having a repulsive interatomic interaction. We should also mention that the realization of two- and three-dimensional optical lattices [6, 31] opens the possibility to study discrete/nonlinear effects in higher spatial dimensions. A discussion of the derivation of the generalized DNLS equation is presented in Section II.

In free space, the superflow of a uniform BEC is described by plane waves, which becomes energetically unstable in presence of defects when the BEC velocity is faster than sound, which is the Landau criterion for superfluidity. The propagation of sound in a harmonically trapped condensate without OL has been observed experimentally [32] and studied theoretically [33, 34, 35, 36]. In the presence of a periodic potential, the condensate wavefunction can be expanded in Bloch waves, having amplitudes modulated with the periodicity of the OL, which can also become energetically unstable when the group velocity is larger than the sound velocity [17, 20, 37, 38, 39, 40]. The energetic instability manifests itself with the emission of quasi-particles out of a condensate flowing against a small obstacle. This happens when the condensate velocity is larger than a critical value, which, in the limit of small obstacles is the sound velocity. The interplay between discreteness and nonlinearity is also crucial for the occurrence of modulational instabilities (MI), well known in the theory of nonlinear media. MI are dynamical instabilities characterized by an exponential growth of arbitrarily small fluctuations of a carrier wave, as a result of the interplay between dispersion and nonlinearity. The consequences of the modulational instability of the motion of BEC wavepackets in OL have been discussed in [41]. A different parametric instability, which will not be discussed here, can arise when modulating in time the height of the interwell barriers or the strength of the interparticle interaction [42, 43]. In Section III we will discuss the excitation spectra of a BEC in a periodic potential, while in Section IV we review the occurrence of a discrete modulational instability, comparing its effects with those of the Landau instability; a brief discussion of the the propagation of sound in the OL will be also presented. A discussion of the dynamics of BEC wavepackets in OL is given in Section V.

At last (but not at least) the high laser power available nowadays allows for the investigation of low tunneling rates between adjacent wells of the periodic potential: in these regimes the quantum fluctuations play an important role, and, with a strength of the optical potential V_0 large enough, it is expected a quantum transition from a superfluid phase to a Mott insulator phase. The model used to

describe the quantum (beyond Gross-Pitaevskii) properties of ultracold atoms in deep optical lattices is the Bose-Hubbard Hamiltonian, which is nothing less than the quantized version of the DNLS Hamiltonian. The basic energy scales in the Bose-Hubbard model are the tunneling energy K (which decreases by increasing V_0) and the charging energy U_2 , due to the interaction among particles in the same well. Since the role of the quantum fluctuations depends on the ratio U_2/K , the OL provide an unique way to tune the effective interaction by varying the laser power V_0 . The phase structure is determined by the two competing terms of the Hamiltonian [44]: the interaction energy U_2 leads to localization of particles in the lattice (Mott phase), while the hopping term K favors superfluidity. The phase coherence of different condensates in the superfluid phase (and its disappearance in the Mott regime) in the array plays a crucial role in the dynamics, and can be experimentally studied observing the interference patterns created by the condensates after turning off the trapping potential. The observation of squeezed number states was reported in [45], while an experimental detection of the Mott-superfluid transition has been reported for 3D OL in [31]. A systematic study of quantum phase transitions in low-dimensional (1D and 2D) OL is presented in [46]. We also mention that adding a disordered potential - created e.g. by an optical speckle potential [47, 48, 49] or by superimposing laser with different periodicity [50, 51] - one expects, in presence of deep optical lattices and for large values of U_2/K , a Bose glass phase [44]. For space reasons, we will not discuss here the main properties of the Bose-Hubbard Hamiltonian and we refer the reader to the chapter devoted to beyond Gross-Pitaevskii effects.

2 Discrete Equations for the Dynamics

The $T = 0$ dynamics of a BEC in an external potential $V(\mathbf{r})$ follows the GPE [52, 53, 54, 55]

$$i\hbar\psi_t = -\frac{\hbar^2}{2m}\nabla^2\psi + [V + g|\psi|^2]\psi, \quad (1)$$

where $g = 4\pi\hbar^2 a/m$, with a the s -wave scattering length and m the atomic mass. The condensate wave function is normalized to the total number of particles N . We write the external potential $V = V_{\text{MT}} + V_{\text{OL}}$ as the sum the optical lattice potential V_{OL} , created by two or more counterpropagating laser beams, and the trap potential V_{MT} , whose form depends on the particular realization of the experiment. For a 1D OL, created by only two counterpropagating laser beams, it is $V_{\text{OL}}(\mathbf{r}) = V_L(y, z) \cos^2(2\pi x/\lambda)$, where $\lambda = \lambda_{\text{laser}} \sin(\theta/2)$, λ_{laser} being the wavelength of the lasers and θ the angle between the counterpropagating laser beams. The spacing in the lattice is $d = \lambda/2$ and $V_L(y, z)$ is determined by the transverse intensity profile of the (nearly gaussian) laser beams. E.g., in [4], $\lambda = 850 \text{ nm}$ and the $1/e^2$ radius of the transverse profile is $\approx 80 \mu\text{m}$, an order of magnitude larger than the transverse radius of the condensate, so that we can approximate the periodic potential by

$$V_{\text{OL}}(x) = V_0 \cos^2(k_x x) \quad (2)$$

where $k_x = 2\pi/\lambda$, V_0 is the trap depth at the center of the beam, and $V_0 = sE_R$ where $E_R = \hbar^2 k_x^2 / 2m$ is the recoil energy. A 2D (3D) OL reads $V_{\text{OL}}(x, y) = V_0 [\cos^2(k_x x) + \cos^2(k_y y)]$ ($V_{\text{OL}}(\mathbf{r}) = V_0 [\cos^2(k_x x) + \cos^2(k_y y) + \cos^2(k_z z)]$). For the 1D periodic potential (2) it is useful to write $V(\mathbf{r}) = V_D(x) + V_L(\mathbf{r})$, where $V_D(x)$ is the x component of the potential $V_{\text{MT}} \equiv V_x(x) + V_y(y) + V_z(z)$. V_D has a simple physical meaning: $F = -\frac{\partial V_D}{\partial x}$ is the effective force acting on the center of mass of a condensate wave packet moving in the periodic potential.

When the laser power (i.e. V_0) is large enough, we can use a tight-binding approximation and decompose the condensate order parameter $\psi(\mathbf{r}, t)$ as a sum of wave functions $\Phi(\mathbf{r} - \mathbf{r}_j)$ localized in each well of the periodic potential:

$$\psi(\mathbf{r}, t) = \sum \psi_j(t) \Phi(\mathbf{r} - \mathbf{r}_j), \quad (3)$$

where we denote by j the different wells in the array and $\psi_j(t) = \sqrt{N_j(t)} e^{i\phi_j(t)}$ is the j -th amplitude. Normalizing to 1 the Φ 's, it follows $\sum_j |\psi_j|^2 = N$.

By replacing ansatz (3) in (1), the GPE reduces to a DNLS equation [22]:

$$i\hbar \frac{\partial \psi_j}{\partial t} = -K(\psi_{j-1} + \psi_{j+1}) + \epsilon_j \psi_j + U_2 |\psi_j|^2 \psi_j, \quad (4)$$

where the tunneling rate is

$$K \simeq - \int d\mathbf{r} \left[\frac{\hbar^2}{2m} \nabla \Phi_j \cdot \nabla \Phi_{j+1} + \Phi_j V \Phi_{j+1} \right], \quad (5)$$

the on-site energies are $\epsilon_n = \int d\mathbf{r} \left[\frac{\hbar^2}{2m} (\nabla \Phi_n)^2 + V \Phi_n^2 \right]$ and the nonlinear coefficient (which we will suppose equal in each site) is

$$U_2 = gN \int d\mathbf{r} \Phi_n^4. \quad (6)$$

Naturally, if one has a 2D (3D) OL, then the ansatz (3) would lead to a 2D (3D) DNLS equation. Equation (4) is the equation of motion $\dot{\psi}_j = \frac{\partial \mathcal{H}}{\partial (i\hbar \psi_j^*)}$, where \mathcal{H} is the Hamiltonian function

$$\mathcal{H} = -K \sum (\psi_j \psi_{j+1}^* + \psi_j^* \psi_{j+1}) + \sum \left(\epsilon_j |\psi_j|^2 + \frac{U_2}{2} |\psi_j|^4 \right). \quad (7)$$

Both the Hamiltonian \mathcal{H} and the normalization are conserved.

In the tight-binding ansatz (3) one includes only corrections from the first band, which is correct for large V_0 . For V_0 intermediate is useful to introduce contributions from the higher bands, i.e. by considering the ansatz $\psi(\mathbf{r}, t) = \sum_{j,\gamma} \psi_{j,\gamma}(t) \Phi_\gamma(\mathbf{r} - \mathbf{r}_j)$, where γ labels the bands: a discussion of the resulting discrete vector equation is presented in [28]. We also notice that the DNLS equation for just two sites describes the dynamics of BEC in a double well, which reduces to the dynamics of a non-rigid pendulum [56, 57, 58]: the dynamical splitting of a BEC into two parts has been experimentally studied in [59, 60], while the direct observation of the atomic tunneling in a BEC double well has been reported in [61].

2.1 Effects of Transverse Confinement

The assumption (3) firstly relies on the fact that the interwell barrier V_0 is much higher than the chemical potentials (e.g., in [9] for $V_0 \sim 5E_R$ it is $\mu \sim 0.1V_0$). A second important condition is that the energy of the system should be confined within the lowest band. Higher energy bands are not contained in the DNLS equation, and become important when the energy is of the order of $\hbar\omega$, where ω is the harmonic frequency of a single well of the lattice. The effective dimensionality of the BEC's trapped in each well can also play a crucial role [62, 30], by modifying the degree of nonlinearity of the DNLS equation. In this prospect, the DNLS equation can be seen as a zero-order (perturbative) approximation of more complicated discrete, nonlinear equations.

The density profile of each condensate can strongly depend on the number of atoms present at a given instant in the same well. This introduces site- and time-dependent parameters in the DNLS Eq. (4), modifying, in particular, its effective degree of nonlinearity. The tight-binding approximation of nonlinear systems has to be generalized as [30]

$$\psi(\mathbf{r}, t) = \sum \psi_j(t) \Phi_j(\mathbf{r}; N_j(t)), \quad (8)$$

with $\Phi_j(\mathbf{r}; N_j(t))$ depending *implicitly* on time through $N_j(t) \equiv |\psi_j(t)|^2$. We stress here, and discuss again later, that the spatial wavefunctions Φ_j (which are considered sufficiently localized in each well) can also depend *explicitly* on time due to the excitation of internal modes. For typical experimental setups, however, we can consider the adiabatic limit in which the interwell number/phase dynamics is much slower than the typical time associated with the excitations of such internal modes (and, of course, the cases where such modes are not already present in the initial configuration of the system). In this limit, which can be well satisfied in experiments, the spatial wavefunctions in Eq. (8) will adiabatically follow the tunneling dynamics and can be approximated with the *real* wavefunction $\Phi_j(\mathbf{r}; N_j(t))$. A discussion of the validity of the adiabatic approximation is in [30].

Replacing the nonlinear tight-binding approximation (8) in the GPE (1) and integrating out the spatial degrees of freedom one finds the following discrete nonlinear equation (DNL) [30]:

$$i\hbar \frac{\partial \psi_j}{\partial t} = -\chi [\psi_j(\psi_{j+1}^* + \psi_{j-1}^*) + c.c.] \psi_j + \epsilon_j \psi_j + \mu_j^{loc} \psi_j - [K + \chi (|\psi_j|^2 + |\psi_{j+1}|^2)] \psi_{j+1} - [K + \chi (|\psi_j|^2 + |\psi_{j-1}|^2)] \psi_{j-1}. \quad (9)$$

In Eq. (9), the ‘‘local’’ chemical potential is the sum of three contributions

$$\mu_j^{loc} = \int d\mathbf{r} \left[\frac{\hbar^2}{2m} (\nabla \Phi_j)^2 + V_L \Phi_j^2 + g|\psi_j|^2 \Phi_j^4 \right]. \quad (10)$$

μ_j^{loc} depends on the atom number N_j through the condensed wavefunction Φ_j . The tunneling rates $K_{j,j\pm 1}$ between the adjacent sites j and $j \pm 1$ also depend, in principle, on the respective populations: expanding the wavefunctions around

an average number of atoms per site, N_0 , and keeping only the zero order term $\Phi_j(N_j) \simeq \tilde{\Phi}_j(N_0)$ one finds $K_{j,j\pm 1} \approx K$, with K given by Eq. (5). The relative error committed in this approximation is order of 10^{-4} for typical experimental setups. The coefficient χ is given by

$$\chi = -g \int d\mathbf{r} \tilde{\Phi}_j^3 \tilde{\Phi}_{j\pm 1}. \quad (11)$$

The on-site energies arising from any external potential superimposed to the OL are $\epsilon_j = \int d\mathbf{r} V_D \Phi_j^2$: $\epsilon_j \propto j^2$ ($\epsilon_j \propto j$) when the driving field is harmonic (linear) - moreover ϵ_j does not depend on the on-site atomic populations. Numerical estimates show that spatial integrals involving next-nearest-neighbor condensates, as well as terms proportional to $\int d\mathbf{r} \Phi_j^2 \Phi_{j\pm 1}^2$, can be neglected, but not the terms proportional to χ . E.g., setting $\zeta = g \int d\mathbf{r} \tilde{\Phi}_j^2 \tilde{\Phi}_{j\pm 1}^2$ one has - for $V_0 \approx 20E_R$ and $N_0 \approx 10000$ - $\chi N_0/K \sim 10^{-1}$ and $\zeta N_0/K \sim 10^{-4}$. In a double well potential e.g., with height barrier $V_0 \approx 2\pi \cdot 500Hz$ and $N_0 \approx 3000$, one has $\chi N_0/K \sim 1$, while $\zeta N_0/K \sim 10^{-3}$. For these reasons, one cannot neglect the χ terms in Eq. (9). Further studies of a BEC in a double well potential without neglecting terms proportional to $\int d\mathbf{r} \Phi_j^2 \Phi_{j\pm 1}^2$ are presented in [63, 64].

To make Eq. (9) useful, one has to guess the dependence of the localized wavefunction Φ_j on N_j . It turns out that a reasonable choice is given by supposing a Thomas-Fermi expression for the Φ_j 's: to be more explicit, let us introduce the potential \tilde{V} at the bottom of wells, obtained expanding the potential V around the minima. At the lowest order $\tilde{V} \approx (m/2)(\tilde{\omega}_x^2 x^2 + \tilde{\omega}_y^2 y^2 + \tilde{\omega}_z^2 z^2)$. One has to compare the interaction energy with the frequencies $\tilde{\omega}_{x,y,z}$: we denote by $\mathcal{D} = 0, 1, 2, 3$ the *number* of spatial dimensions in which one can use the Thomas-Fermi approximation. E.g., $\mathcal{D} = 3$ means that we can approximate Φ_j with the Thomas-Fermi expression $\tilde{\Phi}_j(\mathbf{r}; N_j) \propto (\tilde{\mu}_j - \tilde{V}(\mathbf{r}))$ where $\tilde{\mu}_j$ is fixed by the normalization condition and depends on N_j - with $\mathcal{D} = 2$, denoting by (let say) y and z the directions in which one can apply the Thomas-Fermi expression, one can factorize $\Phi_j = \phi_j(x)\phi_{TF}^{(j)}(y, z)$ with the Thomas-Fermi expression $\phi_{TF}^{(j)}(y, z; N_j) \propto (\tilde{\mu}_j - (m/2)(\tilde{\omega}_y^2 y^2 + \tilde{\omega}_z^2 z^2))$, $\tilde{\mu}_j$ yet being determined by the normalization of the Φ_j . Proceeding along this way, one gets [30]

$$\mu_j^{loc} = U_\alpha |\psi_j|^\alpha; \quad \alpha \equiv \frac{4}{2 + \mathcal{D}}. \quad (12)$$

The coefficient U_α is obtained from Eq.(10) and depends in general on the specific trap potential. An estimate for it in a particular setup is given below in Eq.(14). The DNLS Eq. (4) is recovered from the DNL Eq. (9) in the case $\mathcal{D} = 0$ (i.e. $\alpha = 2$) and neglecting terms proportional to χ . In conclusion the main effect of the transverse confinement is to change the degree of nonlinearity and the generalized DNLS equation reads

$$i\hbar \frac{\partial \psi_j}{\partial t} = -K(\psi_{j-1} + \psi_{j+1}) + \epsilon_j \psi_j + U_\alpha |\psi_j|^\alpha \psi_j - \chi \mathcal{F} \quad (13)$$

where $\mathcal{F} \equiv [\psi_j(\psi_{j+1}^* + \psi_{j-1}^*) + c.c.] \psi_j + (N_j + N_{j+1})\psi_{j+1} + (N_j + N_{j-1})\psi_{j-1}$.

To make the previous result more transparent, let us consider an harmonic trap potential $V_{\text{MT}} = (m/2)(\omega_x^2 x^2 + \omega_y^2 y^2 + \omega_z^2 z^2)$. When the Φ_j does not depend on N_j , one has $\mathcal{D} = 0$ and $\alpha = 2$, as in the standard DNLS equation. However, for deep 1D lattices, the effective frequencies in the x direction is given by $\tilde{\omega}_x = \sqrt{2V_0 k_x^2/m}$ and is $\tilde{\omega}_x \sim 10kHz$ for $V_0 \sim 5E_R$, while $\omega_{x,y,z}/2\pi \sim 100Hz$, for ^{87}Rb . Then, for a number of particles $\sim 1000 - 10000$ one can use a Thomas-Fermi dependence on N_j for the wavefunctions in the y and z directions, but not in the x direction: with the previous notation, this means $\mathcal{D} = 2$ and $\alpha = 1$. This result can be simply obtained by factorizing the localized wavefunction Φ_j as a product of a gaussian ϕ_j having width σ (in the x direction) and a Thomas-Fermi $\phi_{TF}^{(j)}$ (in the y and z coordinates): replacing in Eq. (1) and integrating out along the x direction, one obtains $\epsilon_j = \Omega j^2$, where $\Omega = \frac{m}{2} m \omega_x^2 (\frac{\lambda}{2})^2$, getting the DNL (9) with $\mathcal{D} = 2$ ($\alpha = 1$) and

$$U_1 = \sqrt{m\omega_r^2 g / \sqrt{2\pi}\pi\sigma}. \quad (14)$$

3 Excitation Spectra

In this Section the Bloch and the Bogoliubov excitation spectra of the system in absence of any driving field ($V_L = 0$) are derived in the tight binding approximation. We also present a brief discussion of the comparison with numerical results for the excitation spectra of the continuous GPE [20].

3.1 Bloch Spectrum

The Bloch states $\Psi_p(\mathbf{r}) = e^{ipx/\hbar} \tilde{\Psi}_p(\mathbf{r})$, where $\tilde{\Psi}_p(\mathbf{r})$ is periodic in the x direction with period d , are exact stationary solutions of the Gross-Pitaevskii equation (1). The energy per particle $\epsilon_\gamma(p)$ (Bloch energy) and the chemical potential $\mu_\gamma(p)$ of such solutions form a band structure, so that they can be labeled by the quasi-momentum p and the band index γ .

The generalized DNLS equation (13) describes only the lowest band of the spectrum. Exact solutions of the DNL equation are the "plane waves" $\psi_j = \psi_0 e^{i(kj - \mu t)/\hbar}$, where $p = \hbar k/d$ is the quasi-momentum. Note that the ψ_j are plane waves in the lattice, but do not correspond to plane waves in real space. Within the DNL equation framework, the energy per particle $\epsilon(k)$ and chemical potential $\mu(k)$ corresponding to these solutions are found to be [20]

$$\epsilon(k) = \epsilon^{loc} - 2(K + 2\chi N_0) \cos(k) = \epsilon^{loc} - \frac{\hbar^2}{d^2 m_\epsilon} \cos(k), \quad (15)$$

$$\mu(k) = \mu^{loc} - 2(K + 4\chi N_0) \cos(k) = \mu^{loc} - \frac{\hbar^2}{d^2 m_\mu} \cos(k), \quad (16)$$

where $\epsilon^{loc} = 2U_\alpha N_0^{\alpha/2}/(\alpha + 2)$ and $\mu^{loc} = \mu_j^{loc}|_{\psi_l = \psi_0} = \partial(N_0 \epsilon^{loc})/\partial N_0$, with $N_0 = |\psi_0|^2$ the number of atoms per well. In the previous equations we have introduced

the effective masses m_ε and m_μ , to emphasize the low momenta (long wavelength) quadratic behaviour of the Bloch energy spectrum and of the chemical potential [21]. It turns out that several dynamical properties of the system can be intuitively understood in terms of such effective masses. This approach is quite common, for instance, in the theory of metals, where $m_\mu \equiv m_\varepsilon$. However in BEC, because of the nonlinearity of the Gross-Pitaevskii equation, the two relevant energies of the system, ε and μ , have the same $\cos(k)$ dependence on the quasi-momentum p , but different curvatures. Therefore, $m_\mu \neq m_\varepsilon$, with

$$\frac{1}{m_\varepsilon} \equiv \left. \frac{\partial^2 \varepsilon}{\partial p^2} \right|_0 = \frac{2d^2 (K + 2 \chi N_0)}{\hbar^2}, \quad \frac{1}{m_\mu} \equiv \left. \frac{\partial^2 \mu}{\partial p^2} \right|_0 = \frac{2d^2 (K + 4 \chi N_0)}{\hbar^2}. \quad (17)$$

It is possible to extend the definition of the effective masses to the full Brillouin zone, introducing the quasi-momentum dependent masses $m_\varepsilon(k) \equiv (\partial^2 \mu / \partial p^2)^{-1} = m_\varepsilon / \cos(k)$ and $m_\mu(k) \equiv (\partial^2 \mu / \partial p^2)^{-1} = m_\mu / \cos(k)$, where $m_\varepsilon \equiv m_\varepsilon(0)$ and $m_\mu \equiv m_\mu(0)$.

Similarly, one can introduce two different group velocities, defined as

$$v_\varepsilon \equiv \frac{\partial \varepsilon}{\partial p} = \frac{1}{m_\varepsilon} \frac{\hbar}{d} \sin(k), \quad v_\mu \equiv \frac{\partial \mu}{\partial p} = \frac{1}{m_\mu} \frac{\hbar}{d} \sin(k). \quad (18)$$

These two different group velocities are related by [20, 21] $v_\mu = v_\varepsilon + \frac{\partial v_\varepsilon}{\partial N_0} N_0$ with, given Eqs. (17), $v_\mu > v_\varepsilon$. The current carried by a Bloch waves with quasi-momentum p is $\rho_0 v_\varepsilon(p)$, where ρ_0 is the average particle density; m_μ , on the other hand, plays a crucial role in the Bogoliubov spectrum, which we will discuss below.

The concept of effective mass, defined as the inverse of the curvature of the corresponding spectrum (as that of *group velocity*, defined as the first derivative) can be extended to shallow OL, where the nonlinear tight binding approximation breaks down. In this case, the quasi-momentum dependence of ε and μ will not be simply described by a cosine function, but will still remain periodic in the quasi-momentum p . In particular, the value k where $m_\varepsilon(p)$ changes sign (corresponding to $\partial^2 \varepsilon / \partial p^2 = 0$) will be greater than $\pi/2$ and will in general not coincide with the momentum where m_μ changes sign (corresponding to $\partial^2 \mu / \partial p^2 = 0$).

We remark that the Bloch states are not the only stationary solutions of the Gross-Pitaevskii equation. Because of nonlinearity, indeed, periodic solitonic solutions can also appear for a weak enough periodic potential, introducing new branches in the excitation spectra [65].

3.2 Bogoliubov Spectrum

In this subsection we study the Bogoliubov spectrum of elementary excitations. This describes the energy of small perturbations with quasi-momentum q on top of a macroscopically populated state with quasi-momentum p [stationary solution of Eq. (1)].

We consider first the case $\chi = 0$: in the homogeneous limit ($\epsilon_j = 0$), the stationary solutions of Eq. (13) are plane waves $\psi_j(t) = \psi_0 \exp[i(kj - \nu t)]$,

with frequency ν given by $\hbar\nu = -2K \cos(k) + U|\psi_0|^\alpha$. The stability analysis of such states can be carried out by perturbing the carrier wave as $\psi_j(t) = (\psi_0 + u(t)e^{iqj} + v^*(t)e^{-iqj})e^{i(kj-\nu t)}$. Retaining only terms proportional to u/ψ_0 and v/ψ_0 , one gets

$$i\hbar \frac{d}{dt} \begin{pmatrix} u \\ v \end{pmatrix} = \begin{pmatrix} \mathcal{A} & \mathcal{C} \\ -\mathcal{C}^* & -\mathcal{A} \end{pmatrix} \begin{pmatrix} u \\ v \end{pmatrix} = \hbar\omega_\pm \begin{pmatrix} u \\ v \end{pmatrix}. \quad (19)$$

with $\mathcal{A} = 2K \cos(k) - 2K \cos(k+q) + (1/2)U\alpha|\psi_0|^\alpha$ and $\mathcal{C} = (1/2)U\alpha\psi_0^{*\alpha/2-1}\psi_0^{\alpha/2+1}$ [20]. From Eq. (19) it follows that the excitation spectrum (i.e., the Bogoliubov dispersion relation) for the DNLS with nonlinearity degree α is:

$$\omega_\pm/2K = \sin(k)\sin(q) \pm \sqrt{4\cos^2(k)\sin^4\left(\frac{q}{2}\right) + \frac{\alpha U}{K}|\psi_0|^\alpha \cos(k)\sin^2\left(\frac{q}{2}\right)}. \quad (20)$$

The carrier wave becomes modulationally unstable when the eigenfrequency ω in Eq. (20) becomes imaginary: the condition for stability is

$$4K \cos^2(k)\sin^2\left(\frac{q}{2}\right) + \alpha U|\psi_0|^\alpha \cos(k) > 0. \quad (21)$$

When U is negative (positive), corresponding to negative (positive) scattering length, the plane waves with $\cos(k) < 0$ ($\cos(k) > 0$) are stable. When the lhs side of Eq. (21) becomes negative, as a consequence of the fact that eigenfrequency ω in Eq. (20) becomes imaginary, there is an exponential growth of small perturbations of the carrier wave: we refer to this instability as the modulational instability.

In the general case $\chi \neq 0$ one can repeat the previous stability analysis getting [20]

$$\hbar\omega_\pm \approx \frac{\hbar^2 \sin(k)\sin(q)}{m_\mu d^2} \pm 2\sqrt{\frac{\hbar^4 \cos^2(k)\sin^4(q)}{m_\mu^2 d^4} + \frac{\hbar^2 N_0}{m_\varepsilon d^2} \frac{\partial \mu}{\partial N_0} \cos(k)\sin^2(q)} \quad (22)$$

with the chemical potential given by $\mu = \mu^{loc} - \frac{\hbar^2}{d^2 m_\mu} \cos(k)$ (see Eq. (16)), and $\mu^{loc} = U_\alpha |\psi_0|^\alpha$. For $\alpha = 2$ (i.e. $\mathcal{D} = 0$) and in the limit $\chi = 0$, we recover the well known results for the discrete nonlinear Schrödinger equation [66].

4 Landau and Dynamical Instabilities

From the relation (22), valid for the DNL (13) with $\chi \neq 0$, the small q (large wavelength) limit of the Bogoliubov dispersion relation becomes

$$\hbar\omega \approx \frac{\hbar}{dm_\mu} \sin(k) q + |q| \sqrt{\frac{1}{m_\varepsilon} \frac{\partial \mu}{\partial N_0} N_0 \cos(k)}, \quad (23)$$

(we assume, for the moment, that $\frac{1}{m_\varepsilon} \frac{\partial \mu}{\partial N_0} N_0 \cos(k) > 0$). The linear behaviour in q indicates that the system supports (low amplitude) sound waves, propagating on top of large amplitude traveling waves with velocity

$$v_{s,\pm} = \hbar \frac{\partial \omega}{\partial q} \Big|_{q \rightarrow 0^\pm} = \begin{cases} v_\mu + c, & (q \rightarrow 0^+) \\ v_\mu - c, & (q \rightarrow 0^-) \end{cases} \quad (24)$$

where the ‘‘chemical potential group velocity’’ v_μ has been defined in Eq. (18), and the ‘‘relative sound velocity’’ c is defined as

$$c = \sqrt{\frac{1}{m_\varepsilon} \frac{\partial \mu}{\partial N_0} N_0 \cos(k)}. \quad (25)$$

The two velocities $v_{s,\pm}$ correspond, respectively, to a sound wave propagating in the same and in the opposite direction of the large amplitude traveling wave.

We remark that, contrary to the case of a Galilean invariant system ($s = 0$), the sound velocity depends on the quasi-momentum p . Moreover, v_s depends on the effective dimensionality of the condensates, since (cf. Eqs. (12) and (16)) $\frac{\partial \mu}{\partial N_0} N_0 \sim \alpha U_\alpha N_0^{\alpha/2}$. In the limit $\alpha = 2$, $p \rightarrow 0$ and $m_\varepsilon, m_\mu \rightarrow m$ we get the sound velocity in the uniform case.

The system is energetically unstable if there exists an $\omega < 0$. In the limit $s = 0$, this corresponds to a group velocity larger than the sound velocity (Landau criterion for superfluidity). When the system has a discrete translational invariance ($s > 0$) the condition for this instability is obtained from the Bogoliubov excitation spectrum Eq. (22). Then, we have that the system is not superfluid when $\omega < 0$, corresponding to $v_\mu^2 > c^2$. This result should be compared with the well known Landau criterion for an homogeneous system ($s = 0$), stating that the superfluid is energetically unstable when $v^2 > c^2$, $v \equiv \frac{\partial \varepsilon}{\partial p} = \frac{\partial \mu}{\partial p}$ being the group velocity of the condensate, and $c = \sqrt{\frac{1}{m} \frac{\partial \mu}{\partial N_0} N_0}$ the sound velocity.

There is a further dynamical (modulational) instability mechanism associated with the appearance of an imaginary component in the Bogoliubov frequencies, which disappears in the absence of interatomic interactions, or in the translational invariant limit (if $a > 0$). The onset of this instability in the tight binding regime, coincides with the condition

$$c^2 < 0 \Rightarrow \cos(k) < 0 \Rightarrow |k| > \frac{\pi}{2}. \quad (26)$$

The dynamical instability drives an exponentially fast increase of the amplitude of the - initially small - fluctuations of the condensate (while the energetic instability should manifest itself in polynomial time [67]). Since the initial phases and amplitudes of the fluctuation modes are essentially random, their growth induce a strong dephasing of the condensate, and dissipates its translational kinetic energy (which is transformed in incoherent collective and single particles excitations). We remark here the different scaling of the energetic and dynamical instability with the interatomic interactions. Decreasing the scattering length, the sound velocity decreases, and smaller and smaller group velocities can break down the superfluidity of the system (when $a \rightarrow 0$, the sound velocity $c \rightarrow 0$: in the limit of vanishing interactions the condensate is energetically unstable for an arbitrary small group velocity). On the other hand, the dynamical modulational instability criterion does

not depend on the scattering length. This apparent paradox is simply solved noticing that the growth time of the unstable modes actually depends on interactions, and diverges when the scattering length vanishes ($\tau \rightarrow \infty$ when $a \rightarrow 0$). Therefore, a noninteracting condensate is always dynamically stable. There is a further point to remark: if we consider a condensate moving with an increasing velocity, the system always becomes first energetically unstable, then it hits the dynamical instability. As a matter of fact, however, in real experiments the energetic instability can grow quite slowly (and at zero temperature only in presence of impurities [17]), so that the dominant dephasing mechanism is given by the modulational instability.

5 Wave-Packet Dynamics

In this Section we review the main properties to the wave-packet dynamics of a BEC in an OL, summarizing here the results of a variational approach, previously considered in [22, 30]. The approach uses a general variational wavefunction

$$\psi_j = \sqrt{\mathcal{K}(\sigma)} f\left(\frac{j-\xi}{\sigma}\right) e^{ip(j-\xi) + i\frac{\delta}{2}(j-\xi)^2} \quad (27)$$

where $\xi(t)$ and $\sigma(t)$ are, respectively, the center and the width of the wavepacket, $p(t)$ and $\delta(t)$ their associated momenta and $\mathcal{K}(\sigma)$ a normalization factor (such that $\sum_j N_j = N$). f is a generic function, even in the variable $X = (j - \xi)/\sigma$. For simplicity, we will confine ourself to an exponential trial wavefunction $f(X) = e^{-X^2}$ for the standard DNLS equation (4), i.e. $\alpha = 2$ and $\chi = 0$. A discussion of the general case is reported in [41]. The wave packet dynamical evolution can be obtained by using the Euler-Lagrange equations for the Lagrangian $\mathcal{L} = \sum i\hbar\dot{\psi}_j\psi_j^* - \mathcal{H}$, with \mathcal{H} given by Eq. (7). In the following, we rescale the time as $t \rightarrow \hbar t/2K$, measuring the energies in units $2K$. We also set $\Lambda = U_2/2K$ and $E_j = \epsilon_j/2K$. The equations of motion for the variational parameters are [22]

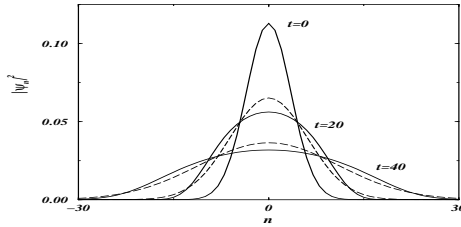
$$\begin{aligned} \dot{p} &= -\frac{\partial\mathcal{V}}{\partial\xi}; \quad \dot{\xi} = \sin p \cdot e^{-\eta}\dot{\delta} = \cos p \left(\frac{4}{\Gamma^2} - \delta^2 \right) e^{-\eta} + \frac{2\Lambda}{\sqrt{\pi}\Gamma^3} - 8\frac{\partial\mathcal{V}}{\partial\Gamma}, \\ \dot{\Gamma} &= 2\Gamma\delta \cos p \cdot e^{-\eta} \end{aligned} \quad (28)$$

where $\Gamma \equiv \sigma^2$, $\eta = 1/2\Gamma + \Gamma\delta^2/8$ and the effective potential \mathcal{V} is given by $\mathcal{V}(\Gamma, \xi) = \mathcal{K} \int_{-\infty}^{\infty} dn E_n \exp(-2(n - \xi)^2/\Gamma)$. The pairs ξ, p and $\frac{\Gamma}{8}, \delta$ are canonically conjugate dynamical variables with respect to the effective Hamiltonian

$$H = \frac{\Lambda}{2\sqrt{\pi}\Gamma} - \cos p \cdot e^{-\eta} + \mathcal{V}(\xi, \Gamma). \quad (29)$$

The effective mass $m^* \equiv m_\epsilon = m_\mu$ (since $\chi = 0$) is given by $\frac{1}{m^*} \equiv \frac{\partial^2 H}{\partial p^2} = \cos p e^{-\eta}$: the quasi-momentum dependence of the effective mass allows a rich variety of dynamical regimes. Solitonic solutions with a positive nonlinear parameter $\Lambda > 0$,

Fig. 1. Plot of the wave function density $\rho_n = |\psi_n|^2$ at times $t = 0, 20, 40$ with $\Lambda = 1$ in the diffusive regime. Numerical values: $p_0 = 0$, $\delta_0 = 0$, $\Gamma_0 = 50$. The critical value of Λ is in this case $\Lambda_c = 24.8$. Solid lines: solutions of Eq. (4) with 73 sites; dashed lines: solutions of variational Eqs. (28).



for instance, are allowed by a negative effective mass. A regime with a diverging effective mass $m^* \rightarrow \infty$ leads to a self-trapping of the wave packet, which has been recently experimentally observed [68].

In the homogeneous lattice, only the optical potential is present ($V_{MT} = V_D = 0$). Therefore the on-site energies E_n , as well as \mathcal{V} , are constant. The momentum is, of course, conserved and it is equal to the initial value: $p(t) = p(0) \equiv p_0$. We will discuss here only the case $\Lambda > 0$, in order to make contact with the experiments in which ^{87}Rb atoms with positive scattering length a are used; however, we observe that the equations of motion (28) are invariant with respect to the replacement $\Lambda \rightarrow -\Lambda$, $p_0 \rightarrow p_0 + \pi$ and $t \rightarrow -t$.

A detailed study of the variational equations of motion is in [69]. Here we quote only the main results and we discuss rather the physical implications and the comparison with a full numerical analysis. This comparison is surprisingly successful in describing even details of the quite complex dynamical and collisional behaviour. Stability phase diagrams for such states are obtained by inspection of the profile dynamics equations [22]. The parameter Λ is the ratio between the nonlinear coefficient, induced by the interatomic interactions, and the coupling between condensates in neighbour wells: it is the only (geometry dependent) parameter which governs the dynamical regimes of the system. When Λ is small, the wave packet spreads out; in the opposite limit, the nonlinearity leads to a localization of the wave packet. When $\cos p_0 < 0$, an intermediate regime arises: in this case, the effective mass is negative and, for a suitable values of Λ , a balance can be reached between nonlinearity and diffusion. In terms of the variational parameters, this means that in the diffusive regime, $\Gamma \rightarrow \infty$ and (if $p_0 \neq 0$) $\xi \rightarrow \infty$, with an effective mass always finite. On the contrary, in the self-trapped regime, Γ remains finite and the center of mass ξ cannot go to ∞ ; furthermore, $1/m^* \rightarrow 0$, meaning that $\eta \rightarrow \infty$ and $\delta \rightarrow \infty$. Therefore in this regime there is an energy transfer to the internal modes of oscillations, since δ is the momentum associated to the wave packet width: in the full numerical solution of Eq. (4), this corresponds to a breakdown of the wave packet. We note that a nonlinear self-trapping occurs also in a two-site model [57, 58, 70].

When $\cos p_0 > 0$, the solitonic regime is forbidden and we have only the diffusive and the self-trapped regimes. In order to show the transition between them, let us consider first the case $p_0 = 0$, in which the center of mass of the wave packet does not move ($\xi = 0$). Using as initial values $\delta_0 = 0$ and Γ_0 , the initial value of the Hamiltonian (29) is $H_0 = \Lambda/2\sqrt{\pi\Gamma_0} - e^{-1/2\Gamma_0}$. Since the Hamiltonian is a conserved quantity, it is $H_0 = \Lambda/2\sqrt{\pi\Gamma} - e^{-1/2\Gamma - \Gamma\delta^2/8}$. Therefore $\frac{\Lambda}{2\sqrt{\pi\Gamma}} - H_0 > 0$:

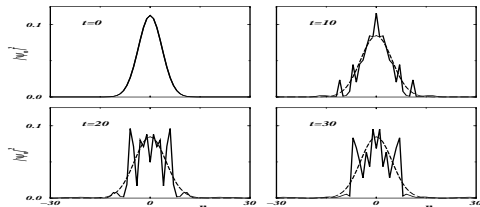


Fig. 2. Plot of the wave function density at times $t = 0, 10, 20, 30$ with $\Lambda = 100$ in the self-trapping region. The numerical values of the remaining parameters are as in Fig. 1.

when $H_0 > 0$, Γ have to remain finite and the we have a self-trapped regime in which the wave packet remains localized and the nonlinearity forbids the diffusion. Vice versa, when $H_0 < 0$, $\Gamma \rightarrow \infty$ for $t \rightarrow \infty$: the wave function spreads out and we are in the diffusive regime. The transition occurs at $H_0 = 0$, with

$$\Lambda_c = 2\sqrt{\pi\Gamma_0}e^{-1/2\Gamma_0}. \quad (30)$$

In Figures 1 and 2 we plot the density $|\psi_n|^2$ for different times with Λ in the diffusive region (Fig. 1) and in the self-trapped one (Fig. 2): the solid lines are the numerical solutions of Eq. (4), the dashed lines are the solutions of the variational equations (28). As we can see from Fig. 2, the numerical solution of Eq. (4) in the self-trapping region loses its gaussian shape [68]. From numerical simulations is also seen that the occurrence of the transition between the diffusive and the self-trapped regimes does not depend on the chosen initial conditions: what is changing is the critical value (30).

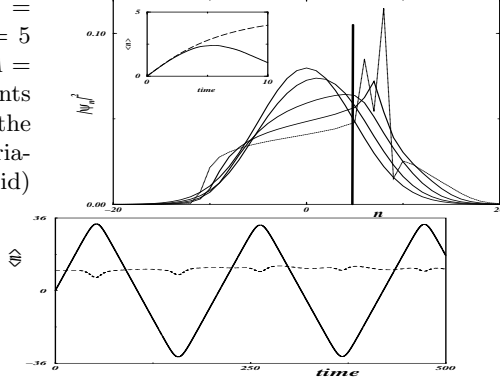
Also when $p_0 \neq 0$, in which the center of the wave packet moves on the lattice, there are two distinct regimes. $H_0 > 0$, i.e., $\Gamma(t) < \Gamma_{max}$ corresponds to the self-trapped regime in which the boson wave packet remains localized around few sites, while a diffusive regime occurs when $-\cos p_0 < H_0 \leq 0$. In this case $\Gamma(t \rightarrow \infty) \rightarrow \infty$ and $\dot{\xi} \approx -H_0/\tan p_0 = \text{const}$. The transition between the regimes occurs at $\Lambda_c = 2\sqrt{\pi\Gamma_0} \cos p_0 e^{-1/2\Gamma_0}$. With $\Lambda > \Lambda_c$, the ratio between the initial value of the width σ_0 and the limit width $\sigma_{max}(t \rightarrow \infty)$ is given by

$$\sigma_0/\sigma_{max} = (\Lambda - \Lambda_c)/\Lambda. \quad (31)$$

We checked the stability of the self-trapping transition also considering different initial forms of the wave packet. In Fig. 3 we consider a self-trapped state ($\Lambda > \Lambda_c$): the variational prediction is that $\dot{\xi} \rightarrow 0$ and that $\xi \rightarrow \text{const}$. As time progresses, the width increases (and it goes asymptotically to a constant value) and the momentum conjugate to the width goes to infinity. The full numerical solution cannot go to this state, because the transfer of energy to the internal state breaks down the wave packet: when the average position approaches to value predicted from the variational analysis (thick line), the wave packet deforms until it breaks. In the inset we compare the numerical and the variational average position, where this deformation determines a deviation between the two lines. We observe that, despite the fact that the variational analysis cannot exactly follow the full dynam-

Fig. 3. Density profiles at times $t = 0, 1.25, 2.5, 3.75$ (solid lines) and at $t = 5$ (dotted) for $p_0 = \pi/4$, $\Gamma_0 = 100$ and $\Lambda = 50$ ($\Lambda_c = 24.8$). The thick line represents the asymptotic value predicted from the variational analysis. In the inset the variational (dashed line) and numerical (solid) average position vs. time are plotted.

Fig. 4. Width (dotted line) and average position (solid line) calculated numerically for $\Lambda = \Lambda_{sol}$ and $p_0 = 3\pi/4$ in a finite array of 73 sites.



ics in the self-trapping, it can, however, predict the occurrence of the transition and give a fairly accurate estimate of the critical point.

For $\cos p_0 < 0$, soliton-like structures are present (cf. [23, 24, 25] for more references on discrete solitons and intrinsic localized excitations). When $\cos p < 0$ the self-trapping condition is given by $H_0 > |\cos p_0|$ and the critical value is

$$\Lambda_c = 2\sqrt{\pi\Gamma_0} |\cos p_0| (1 - e^{-1/2\Gamma_0}). \quad (32)$$

For $\Lambda < \Lambda_c$, $\Gamma \rightarrow \infty$, while for $\Lambda > \Lambda_c$, Γ remains finite. A soliton solution can be determined by imposing $\dot{\Gamma} = \dot{\delta} = 0$. One finds [22]

$$\Lambda_{sol} = 2\sqrt{\pi/\Gamma_0} |\cos p_0| e^{-1/2\Gamma_0}. \quad (33)$$

For $\Lambda = \Lambda_{sol}$ the center of the wave packet moves with a constant velocity $\dot{\xi}$ and its width remains essentially constant in time. We observe that for $\Gamma_0 > 1$, it is $\Lambda_c < \Lambda_{sol}$. In Fig. 4 we plot the average position and the width for $\Lambda = \Lambda_{sol}$. Since we are not using periodic boundary conditions, when the wave packet arrives to the end of the lattice, it hits a wall and upon rebounding, it regains its original shape. For $\Lambda_c < \Lambda < \Lambda_{sol}$, $\xi \rightarrow \infty$ while $\Gamma(t)$ oscillates, corresponding to a breather solution. When $\Gamma_0 > 1$, the breather region extends until $\Lambda_{breath} > \Lambda_{sol}$ [69].

Before concluding, we discuss the relation between the present results and the modulational instability. As we discussed, if we consider a small perturbation on a plane wave $\psi_j \propto e^{ip_0j}$, stability analysis shows that when $\cos p_0 < 0$ the eigenfrequencies of the linear modes become imaginary driving an exponential growth of small perturbations. When $\cos p_0 > 0$, the plane wave is stable. In the present case, we are considering not a plane wave, but a localized wave function; therefore, we may expect to find the result previously stated by considering the case $\Gamma \gg 1$. In this case, when $\cos p_0 > 0$, $\Lambda_c \rightarrow \infty$ and the self-trapped region disappears: this corresponds to the result which there is no modulational instability for $\cos p_0 > 0$. To the contrary, when $\cos p_0 < 0$, then $\Lambda_c \rightarrow 0$ and always the system exhibits instability to small perturbation: this means that we have only self-trapping, as expected.

To conclude this Section, we observe that the variational approach can be applied also in vertical arrays (i.e., when the gravity is acting) when Bloch oscil-

lations occur. Similarly, Bloch oscillations are also possible in horizontal optical lattices realized by two counterpropagating laser beams with a frequency detuning varying linearly in time [8, 71]. The DNLS description of the dynamics is confined to the first band, and then a complete description of the Bloch oscillations in a tilted potential requires the study of the continuous GPE (see [72, 37, 73, 74] and references therein). A discussion on the Landau-Zener tunneling is presented in the following chapter. In an harmonic trap, one can induce and study dipole oscillations suddenly moving the magnetic potential: if the initial trap displacement is smaller than a critical value, it is possible to observe coherent Josephson-like oscillations [9]. When the initial displacement is larger than a critical value, the modulational instability [41] breaks down the dipole oscillations [75].

Acknowledgments: It is a pleasure to thank our colleagues and friends with whom we had pleasant brainstormings. Among the members of the BEC group in Trento, special thanks go to I. Carusotto, F. Dalfovo, S. Giorgini, C. Menotti, L.P. Pitaevskii and S. Stringari. Stimulating discussions with M. Albiez, T. Anker, J. Esteve, R. Gati, and M. Oberthaler are gratefully acknowledged. We also thank L.A. Collins, A.R. Bishop, P.G. Kevrekidis, D.J. Frantzeskakis, S.R. Shenoy, G. Giusiano, F.P. Mancini and P. Sodano and the members of the experimental group at LENS (Florence): F.S. Cataliotti, C. Fort, M. Inguscio, F. Minardi, G. Modugno and M. Modugno.

References

1. I. Bloch, *J. Phys. B* **38**, S629 (2005).
2. D. Jaksch and P. Zoller, *Ann. Phys. (N. Y.)* **315**, 52 (2005).
3. O. Morsch and M.K. Oberthaler, *Rev. Mod. Phys.* **78**, 179 (2006).
4. B.P. Anderson and M.A. Kasevich, *Science* **282**, 1686 (1998).
5. K. Bongs, S. Burger, S. Dettmer, D. Hellweg, J. Arlt, W. Ertmer, and K. Sengstock, *Phys. Rev. A* **63**, 31602 (2001).
6. M. Greiner, I. Bloch, O. Mandel, T.W. Haensch, and T. Esslinger, *Phys. Rev. Lett.* **87**, 160405 (2001).
7. W.K. Hensinger, H. Haffer, A. Browaeys, N.R. Heckenberg, K. Helmerson, C. McKenzie, G.J. Milburn, W.D. Phillips, S.L. Rolston, H. Rubinsztein-Dunlop, and B. Upcroft, *Nature* **412**, 52 (2001).
8. O. Morsch, J.H. Müller, M. Cristiani, D. Ciampini, and E. Arimondo, *Phys. Rev. Lett.* **87**, 140402 (2001).
9. F.S. Cataliotti, S. Burger, C. Fort, P. Maddaloni, F. Minardi, A. Trombettoni, A. Smerzi, and M. Inguscio, *Science* **293**, 843 (2001).
10. B. Eiermann, T. Anker, M. Albiez, M. Taglieber, P. Treutlein, K.P. Marzlin, and M.K. Oberthaler, *Phys. Rev. Lett.* **92**, 230401 (2004).
11. T. Stoferle, H. Moritz, C. Schori, M. Kohl, and T. Esslinger, *Phys. Rev. Lett.* **92**, 130403 (2004).
12. Z. Hadzibabic, S. Stock, B. Battelier, V. Bretin, and J. Dalibard, *Phys. Rev. Lett.* **93**, 180403 (2004).
13. K. Berg-Sorensen and K. Molmer, *Phys. Rev. A* **58**, 1480 (1999).

14. J. Javanainen, Phys. Rev. A **60**, 4902 (1999).
15. D. Choi and Q. Niu, Phys. Rev. Lett. **82**, 2022 (1999).
16. M.L. Chiofalo and M.P. Tosi, Phys. Lett. A **268**, 406 (2000).
17. B. Wu and Q. Niu, Phys. Rev. A **64**, 061603(R) (2001).
18. B. Wu, R. Diener, and Q. Niu, Phys. Rev. A **65**, 025601 (2002).
19. M. Machholm, C.J. Pethick, and H. Smith, Phys. Rev. A **67**, 053613 (2003).
20. C. Menotti, A. Smerzi, and A. Trombettoni, New J. Phys. **5**, 112 (2003).
21. M. Krämer, C. Menotti, L.P. Pitaevskii, and S. Stringari, Eur. Phys. J. D **27**, 247 (2003).
22. A. Trombettoni and A. Smerzi, Phys. Rev. Lett. **86**, 2353 (2001).
23. D. Hennig and G.P. Tsironis, Phys. Rep. **307**, 333 (1999).
24. P.G. Kevrekidis, K.Ø Rasmussen, and A.R. Bishop, Int. J. Mod. Phys. B **15**, 2833 (2001).
25. M.J. Ablowitz, B. Prinari, and A.D. Trubatch, *Discrete and Continuous Nonlinear Schrödinger Systems* (University Press, Cambridge, 2004).
26. F.Kh. Abdullaev, B.B. Baizakov, S.A. Darmanyan, V.V. Konotop, and M. Salerno, Phys. Rev. A **64**, 43606 (2001).
27. V.V. Konotop and M. Salerno, Phys. Rev. A **65**, 021602 (2002).
28. G.L. Alfimov, P.G. Kevrekidis, V.V. Konotop, and M. Salerno, Phys. Rev. E **66**, 046608 (2002).
29. L. Salasnich, A. Parola, and L. Reatto, Phys. Rev. A **65**, 043614 (2002).
30. A. Smerzi and A. Trombettoni, Phys. Rev. A **68**, 023613 (2003).
31. M. Greiner, O. Mandel, T. Esslinger, T.W. Hansch, and I. Bloch, Nature **415**, 39 (2002).
32. M.R. Andrews, D.M. Kurn, H.-J. Miesner, D.S. Durfee, C.G. Townsend, S. Inouye, and W. Ketterle, Phys. Rev. Lett. **79**, 553 (1997).
33. E. Zaremba, Phys. Rev. A **57**, 518 (1998).
34. G.M. Kavoulakis and C.J. Pethick, Phys. Rev. A **58** 1563 (1998).
35. S. Stringari, Phys. Rev. A **58**, 2385 (1998).
36. B. Damski, Phys. Rev. A **69**, 043610 (2004).
37. B. Wu and Q. Niu, New J. Phys. **5**, 104 (2003).
38. E. Taylor and E. Zaremba, Phys. Rev. A **68**, 053611(2003).
39. D. Boers, C. Weiss, and M. Holthaus, Europhys. Lett. **67**, 887 (2004).
40. M. Krämer, C. Menotti and M. Modugno, J. Low Temp. Phys. **138**, 729 (2005).
41. A. Smerzi, A. Trombettoni, P.G. Kevrekidis, and A.R. Bishop, Phys. Rev. Lett. **89**, 170402 (2002).
42. Z. Rapti, P.G. Kevrekidis, A. Smerzi, and A.R. Bishop, J. Phys. B **37**, S257 (2004).
43. M. Krämer, C. Tozzo, and F. Dalfovo Phys. Rev. A **71**, 061602 (2005).
44. M.P.A. Fisher, P.B. Weichman, G. Grinstein, and D.S. Fisher, Phys. Rev. B **40**, 546 (1989).
45. C. Orzel, A.K. Tuchman, M.L. Fenselau, M. Yasuda, and M.A. Kasevich, Science **291**, 2386 (2001).
46. M. Kohl, H. Moritz, T. Stoferle, C. Schori, and T. Esslinger, J. Low Temp. Phys. **138** 635 (2005).
47. J. E. Lye, L. Fallani, M. Modugno, D. S. Wiersma, C. Fort, and M. Inguscio, Phys. Rev. Lett. **95**, 070401 (2005).
48. D. Clément, A.F. Varón, M. Hugbart, J.A. Retter, P. Bouyer, L. Sanchez-Palencia, D.M. Gangardt, G.V. Shlyapnikov, and A. Aspect, Phys. Rev. Lett. **95**, 170409 (2005).

49. T. Schulte, S. Drenkelforth, J. Kruse, W. Ertmer, J. Arlt, K. Sacha, J. Zakrzewski, and M. Lewenstein, *Phys. Rev. Lett.* **95**, 170411 (2005).
50. R. Roth and K. Burnett, *Phys. Rev. A* **68**, 023604 (2003).
51. L. Fallani, J. E. Lye, V. Guarrera, C. Fort, and M. Inguscio, *cond-mat/0603655*.
52. F. Dalfovo, S. Giorgini, L. P. Pitaevskii, and S. Stringari, *Rev. Mod. Phys.* **71**, 463-512 (1999).
53. A.J. Leggett, *Rev. Mod. Phys.* **73**, 307 (2001).
54. C.J. Pethick and H. Smith, *Bose-Einstein Condensation in Dilute Gases* (University Press, Cambridge, 2002).
55. L.P. Pitaevskii and S. Stringari, *Bose-Einstein Condensation* (Oxford University Press, Oxford, 2003).
56. G.J. Milburn, J. Corney, E.M. Wright, and D.F. Walls, *Phys. Rev. A* **55**, 4318 (1997).
57. A. Smerzi, S. Fantoni, S. Giovanazzi, and S.R. Shenoy, *Phys. Rev. Lett.* **79**, 4950 (1997).
58. S. Raghavan, A. Smerzi, S. Fantoni, and S.R. Shenoy, *Phys. Rev. A* **59**, 620 (1999).
59. Y. Shin, M. Saba, T.A. Pasquini, W. Ketterle, D.E. Pritchard, and A.E. Leanhardt, *Phys. Rev. Lett.* **92**, 050405 (2004).
60. T. Schumm, S. Hofferberth, L.M. Andersson, S. Wildermuth, S. Groth, I. Bar-Joseph, J. Schmiedmayer, and P. Kruger, *Nature Phys.* **1**, 57 (2005).
61. M. Albiez, R. Gati, J. Fölling, S. Hunsmann, M. Cristiani, and M.K. Oberthaler, *Phys. Rev. Lett.* **95**, 010402 (2005).
62. P. Pedri, L.P. Pitaevskii, S. Stringari, C. Fort, S. Burger, F.S. Cataliotti, P. Maddaloni, F. Minardi, and M. Inguscio, *Phys. Rev. Lett.* **87**, 220401 (2001).
63. D. Ananikian and T. Bergeman, *Phys. Rev. A* **73**, 013604 (2006).
64. E.W. Kirr, P.G. Kevrekidis, E. Shlizerman, M.I. Weinstein, *nlin.PS/0702038*.
65. M. Machholm, A. Nicolin, C.J. Pethick, and H. Smith, *Phys. Rev. A* **69**, 043604 (2004).
66. Yu.S. Kivshar and M. Peyrard, *Phys. Rev. A* **46**, 3198 (1992).
67. S. Ianeselli, C. Menotti and A. Smerzi, *J. Phys. B* **39**, S135 (2006).
68. T. Anker, M. Albiez, R. Gati, S. Hunsmann, B. Eiermann, A. Trombettoni, and M.K. Oberthaler, *Phys. Rev. Lett.* **94**, 020403 (2005).
69. A. Trombettoni and A. Smerzi, *J. Phys. B* **34**, 4711 (2001).
70. E.A. Ostrovskaja, Yu.S. Kivshar, M. Lisak, B. Hall, F. Cattani, and D. Anderson, *Phys. Rev. A* **61**, R31601 (2000).
71. L. Fallani, L. De Sarlo, J.E. Lye, M. Modugno, R. Saers, C. Fort, and M. Inguscio, *Phys. Rev. Lett.* **93**, 140406 (2004).
72. M. Cristiani, O. Morsch, J.H. Müller, D. Ciampini, and E. Arimondo, *Phys. Rev. A* **65**, 063612 (2002).
73. M. Jona-Lasinio, O. Morsch, M. Cristiani, N. Malossi, J.H. Müller, E. Courtade, M. Anderlini, and E. Arimondo, *Phys. Rev. Lett.* **91**, 230406 (2003).
74. B.M. Breid, D. Witthaut, and H.J. Korsch, *New J. Phys.* **8**, 110 (2006).
75. F.S. Cataliotti, L. Fallani, F. Ferlaino, C. Fort, P. Maddaloni, and M. Inguscio, *New J. Phys.* **5**, 71 (2003).